Catalysis Science & Technology

ROYAL SOCIETY OF CHEMISTRY

PAPER

View Article Online
View Journal | View Issue

Cite this: *Catal. Sci. Technol.*, 2025, **15**, 7059

Confinement-induced *Z*-selectivity in the rhodium *N*-heterocyclic carbene-catalyzed hydroboration of terminal alkynes

Boshra Atwi,[a] Dongren Wang,[a] Johanna R. Bruckner,[b] Wolfgang Frey[c] and Michael R. Buchmeiser *[a]

The N- and O-chelating *N*-heterocyclic carbene (NHC) based Rh(I) and Rh(III) complexes [RhCl(1-(quino-8-yl)-3-(trimethoxysilylpropyl)imidazol-2-ylidene)(COD)] (**Rh1**, COD = 1,5-cyclooctadiene), [RhCl(1-(mesitylaminocarbonylmethyl)-3-(trimethoxysilylpropyl)imidazol-2-ylidene)(COD)] (**Rh2**), [Rh(1-(mesitylaminocarbonylmethyl)-3-(trimethoxysilylpropyl)imidazol-2-ylidene)(COD)$^+$] [BF_4^-] (**Rh3**), [Rh(1-(mesitylamidocarbonylmethyl)-3-(trimethoxysilylpropyl)imidazol-2-ylidene)(COD)] (**Rh4**), RhCl(1-(quino-8-yl)-3-(trimethoxysilylpropyl)imidazol-2-ylidene)(Cp*)$^+$] Cl^- (**Rh5**, Cp* = pentamethylcyclopentadienyl), [RhCl(1-(quino-8-yl)-3-(trimethoxysilylpropyl)imidazol-2-ylidene)(Cp*)$^+$] [BF_4^-] (**Rh6**), [$RhCl_2$(1-(mesitylaminocarbonylmethyl)-3-(trimethoxysilylpropyl)imidazol-2-ylidene)(Cp*)] (**Rh7**), and [RhCl(1-(mesitylaminocarbonylmethyl)-3-(trimethoxysilylpropyl)imidazol-2-ylidene)(Cp*)] [BF_4^-] (**Rh8**) were prepared. The solid-state structures of **Rh3**, **Rh5** and **Rh6** are presented. Selected complexes were used in the hydroboration of terminal aliphatic alkynes under homogeneous conditions using HBpin (pin = pinacolate) as hydroboration reagent. As expected, only very low *β*(*Z*)-selectivity (1–27%) was observed under homogeneous conditions; by contrast, **Rh1**, **Rh4**, **Rh5**, and **Rh7** immobilized inside (hexagonally) ordered mesoporous silica (OMS) with pore sizes of 6.0 and 3.5 nm, respectively, showed improved *β*(*Z*) selectivity up to 30%. Most important, reactions carried out with **Rh1**, **Rh4** and **Rh7** supported on $OMS_{35Å}$ and additionally confined in a thin (1 nm) layer of the ionic liquid 1-butyl-3-methylimidazolium tetrafluoroborate (BMIM$^+$ BF_4^-) using "solid catalyst with ionic liquid layer" (SCILL) conditions allowed for a pronounced increase in *Z*-selectivity up to 67%. Overall, the *β*(*Z*)/*β*(*E*) isomeric ratio was successfully increased up to a factor of 22 when going from homogenous to SCILL conditions. A mechanistic picture is presented.

Received 14th July 2025,
Accepted 7th October 2025

DOI: 10.1039/d5cy00860c

rsc.li/catalysis

1. Introduction

Alkenylboronates are valuable products in organic synthesis, *e.g.* for Suzuki cross-coupling reactions[1,2] and are accessible *via* the direct addition of a hydroborane to a 1-alkyne. This transformation can be accomplished by a metal-catalyzed or metal-free approach.[3] Alkenylboronates are known for their low toxicity and good functional group tolerance[4,5] and can also be transformed into alcohols, amines and halides.[6] Generally, the addition of the hydroboration reagent to an alkyne follows either a Markovnikov or an anti-Markovnikov pathway, potentially forming three different isomers; these are the *α*-, *β*(*Z*)- and the more stable *β*(*E*)-alkenylboronates.[2,7]

Seminal work on the hydroboration of alkynes[6,8–10] has been carried out, notably the work of Brown and Suzuki, as outlined by Carreras *et al.*[2] Since then, a large variety of transition-metal complexes based on Rh, Ir, Co, Cu, Ru, Pd and Pt have been used in the hydroboration of terminal alkynes.[3,8,11–22] Additionally, organo-rare earth metal complexes of Y, La, Nd and Dy were investigated for which excellent *β*(*E*) selectivity was reported.[23] Also, dehydrogenative borylation of alkenes mediated by [Rh(1,5-cyclooctadiene)Cl]$_2$ was reported to provide the *β*(*E*)-alkenylboronates as a main product.[2] Recently, group 4 metal aminophosphine-borane complexes were reported for the hydroboration of alkynes and nitriles with 4,4,5,5-tetramethyl-1,3-dioxa-2-borolane (HBpin) with extraordinary stereoselectivity towards the formation of (*E*)-alkenyl boranes.[3]

Despite all progress in the field, the *selective* formation of *β*(*Z*)-alkenylboronates *via* the hydroboration of terminal alkynes is still challenging and a limited number of studies exist. To be mentioned is the work by Leitner *et al.*, in which high *β*(*Z*)-selectivity was achieved under mild condition using a PNP-based ruthenium hydride catalyst.[24] Regioselective

[a] *Institute of Polymer Chemistry, Universität Stuttgart, Pfaffenwaldring 55, D-70569 Stuttgart, Germany. E-mail: michael.buchmeiser@ipoc.uni-stuttgart.de*
[b] *Institute of Physical Chemistry, Universität Stuttgart, Pfaffenwaldring 55, D-70569 Stuttgart, Germany*
[c] *Institute of Organic Chemistry, Universität Stuttgart, Pfaffenwaldring 55, D-70569 Stuttgart, Germany*

hydroboration of internal alkynes was achieved with a pincer NHC-based Co complexes as well.[25] Beside these reports, Miyaura outlined the selective formation of $\beta(Z)$-alkenylboronates catalyzed by rhodium and iridium complex with additives.[26] In the corresponding work, 3 mol% catalyst loading of $[M(COD)Cl]_2$ (M = Rh or Ir) and a phosphine ligand were tested for the hydroboration of terminal alkynes. As borane sources, both HBpin and HBcat were employed.

Later on, Lyu *et al.* introduced a thioxanthene-based PSP-pincer rhodium catalyst for the highly $\beta(Z)$-selective hydroboration of terminal alkynes. Excellent selectivity was achieved by using a bulky, rigid and electron-rich ligand. A variety of substrates was investigated. Deuterium labeling experiments were performed and a hydroboration mechanism was proposed.[7]

Complementary, bases such as lithium hexamethyldisilazide (LiHMDS), LiO*t*Bu and NaOH have been investigated for their hydroboration ability, too.[27,28] Encouraged by the high *Z*-selectivity in the hydrosilylation of both aromatic and aliphatic alkynes by well-defined Rh-catalysts selectively immobilized inside mesoporous materials,[29] we were interested in investigating the reactivity of Rh(I) and Rh(III) complexes bearing chelating *N*-heterocyclic carbenes (NHCs) in the hydroboration of terminal alkynes under heterogeneous conditions with the catalysts selectively immobilized inside different OMS materials.

2. Results and discussion

Several reports exist on the synthesis of rhodium complexes for hydrosilylation.[30,31] Meanwhile, a series of Rh-NHC complexes by treating NHCs bearing a pendant trimethoxysilyl group with suitable precursors such as $[Rh(COD)Cl]_2$, $[Rh(OMe)(COD)]_2$ or $[Rh(Cp^*)Cl_2]$ were also reported by our group.[29,32] Here, two different NHCs with pendant quinoyl and amido groups were chosen, which allowed for the investigation of the chelating effect on the catalytic reactivity of the complexes in the hydroboration of terminal aliphatic alkynes. [RhCl(1-(quino-8-yl)-3-(trimethoxysilylpropyl) imidazol-2-ylidene)(COD)] (**Rh1**, COD = 1,5-cyclooctadiene) was obtained by deprotonation of the corresponding imidazolium salt with LiHMDS followed by *in situ* addition of $[Rh(COD)Cl]_2$. Reacting the amido-based NHC with Ag_2O in CH_2Cl_2 and further transmetalation using $[Rh(COD)Cl]_2$ yielded [RhCl(1-(mesitylaminocarbonylmethyl)-3-(trimethoxysilylpropyl)imidazol-2-ylidene)(COD)] (**Rh2**). **Rh2** was reacted with $AgBF_4$ in THF to yield the corresponding cationic complex $[Rh(1\text{-}(mesitylaminocarbonylmethyl)\text{-}3\text{-}(trimethoxysilylpropyl)imidazol\text{-}2\text{-}ylidene)(COD)^+][BF_4^-]$ (**Rh3**).

Finally, the N-chelated complex [Rh(1-(mesitylamidocarbonylmethyl)-3-(trimethoxysilylpropyl)imidazol-2-ylidene)(COD)] (**Rh4**) was synthesized in an analogous manner to **Rh2** using $[Rh(OMe)(COD)]_2$ as precursor (Scheme 1).[32] The Rh(III) NHC complexes **Rh5**–**Rh8** were accessible *via* the reaction of the corresponding imidazolium salt with Ag_2O under exclusion of light. Subsequent transmetalation between the silver complexes and 0.5 eq. of $[Rh(Cp^*)Cl_2]_2$ afforded $[RhCl(1\text{-}(quino\text{-}8\text{-}yl)\text{-}3\text{-}(trimethoxysilylpropyl)imidazol\text{-}2\text{-}ylidene)(Cp^*)^+]Cl^-$ (**Rh5**) and $[RhCl_2(1\text{-}(mesitylaminocarbonylmethyl)\text{-}3\text{-}(trimethoxysilylpropyl)imidazol\text{-}2\text{-}ylidene)(Cp^*)]$ (**Rh7**), respectively.

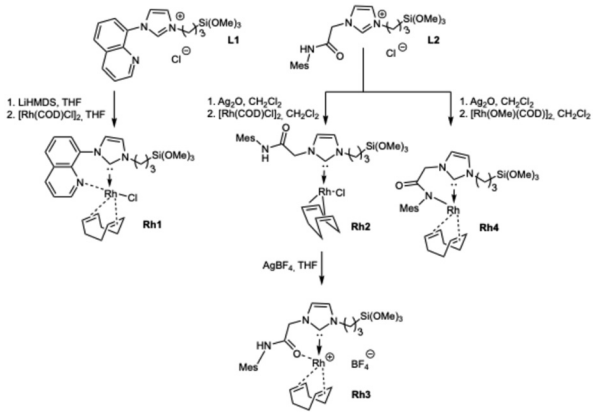

Scheme 1 Synthetic route to the neutral and cationic Rh(I) complexes **Rh1**–**Rh4**.

Further reaction of **Rh5** and **Rh7** with 1 eq. of $AgBF_4$ yielded cationic $[RhCl(1\text{-}(quino\text{-}8\text{-}yl)\text{-}3\text{-}(trimethoxysilylpropyl)imidazol\text{-}2\text{-}ylidene)(Cp^*)^+][BF_4^-]$ (**Rh6**) and $[RhCl(1\text{-}(mesitylaminocarbonylmethyl)\text{-}3\text{-}(trimethoxysilylpropyl)imidazol\text{-}2\text{-}ylidene)(Cp^*)][BF_4^-]$ (**Rh8**) (Cp* = pentamethylcyclopentadienyl) (Scheme 2). The structures of **Rh3**, **Rh5** and **Rh6** were confirmed by single-crystal X-ray analysis (Fig. 1–3).

Rh3 crystallizes in the triclinic space group $P\bar{1}$ with a = 1108.9(2) pm, b = 1216.5(3) pm, c = 1420.1(5) pm, α = 99.026(8)°, β = 101.031(8)°, γ = 116.881(6)°, Z = 2. The Rh center adopts a distorted square planar geometry with the pendant carbonyl group coordinating to the metal (Rh(1)–O(1) 213.4(3) pm). The Rh-NHC distance is 204.0(4) pm. Relevant bond lengths and angles are summarized in Fig. 1. The solid-state structure of cationic **Rh5** is shown in Fig. 2. **Rh5** crystallizes in the monoclinic space group $P2_1/n$ with a =

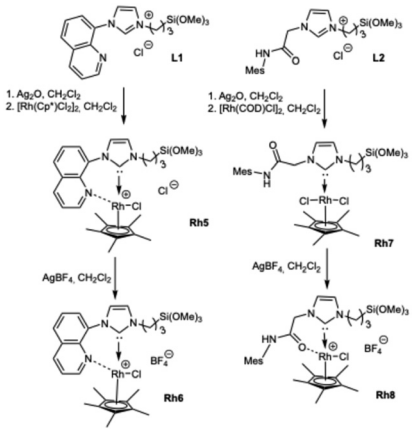

Scheme 2 Synthetic route to the neutral and cationic Rh(III) complexes **Rh5**–**Rh8**.

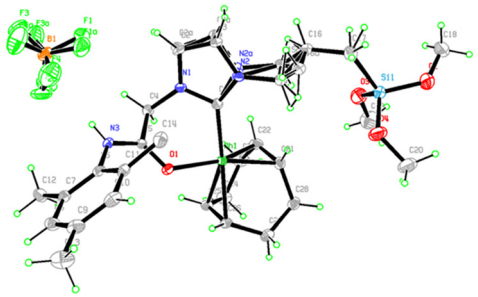

Fig. 1 Molecular structure and selected bond lengths [pm] and angles [°] for **Rh3**: Rh(1)–C(1) 204.0(4), Rh(1)–C(22) 210.6(4), Rh(1)–C(21) 212.2(4), Rh(1)–O(1) 213.4(3), Rh(1)–C(25) 217.0(4), Rh(1)–C(26) 219.9(4); C(1)–Rh(1)–C(22) 91.23(16), C(1)–Rh(1)–C(21) 102.90(16), C(22)–Rh(1)–C(21) 38.70(17), C(1)–Rh(1)–O(1) 84.50(13), C(22)–Rh(1)–O(1) 156.18(15), C(21)–Rh(1)–O(1) 164.53(13), C(1)–Rh(1)–C(25) 150.41(17), C(22)–Rh(1)–C(25) 82.44(16), C(21)–Rh(1)–C(25) 90.11(16), O(1)–Rh(1)–C(25) 89.76(13), C(1)–Rh(1)–C(26) 170.31(15), C(22)–Rh(1)–C(26) 97.33(15), C(21)–Rh(1)–C(26) 81.31(16), O(1)–Rh(1)–C(26) 89.42(12), C(25)–Rh(1)–C(26) 36.63(14). The protons at C(14) were omitted for clarity.

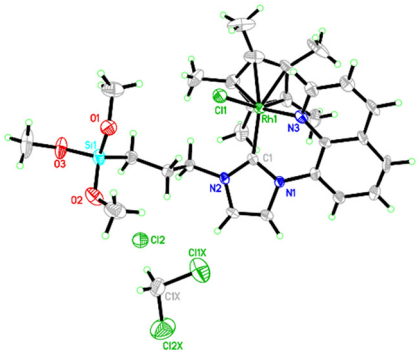

Fig. 2 Molecular structure of **Rh5** with selected bond lengths [pm] and angles [°]: Rh(1)–C(1) 201.0(6), Rh(1)–N(3) 210.7(5), Rh(1)–C(19) 212.8(6), Rh(1)–C(21) 216.5(6), Rh(1)–C(20) 217.7(6), Rh(1)–C(22) 222.1(7), Rh(1)–C(23) 222.9(6), Rh(1)–Cl(1) 240.55(17); C(1)–Rh(1)–N(3) 83.8(2), C(1)–Rh(1)–C(19) 107.1(3), N(3)–Rh(1)–C(19) 101.2(2), C(1)–Rh(1)–C(21) 118.4(3), N(3)–Rh(1)–C(21) 155.9(2), N(3)–Rh(1)–C(20) 138.2(2), C(1)–Rh(1)–Cl(1) 93.27(17), N(3)–Rh(1)–Cl(1) 89.40(14).

715.11(4) pm, b = 1855.98(14) pm, c = 2461.17(18) pm, α = 90°, β = 94.408(3)°, γ = 90°, Z = 4. The Rh-center adopts a three-legged-piano-stool-type geometry. In the solid state, the nitrogen atom of the quinoyl substituent is coordinating to the Rh atom; one chloride forms the counter ion. **Rh5** exhibits a characteristic C(1)–Rh(1)–N(3) angle around 83.8°; the Rh(1)–C(1) bond is 201.0(6) ppm while the Rh(1)–N(3) bond is 210.7(5) ppm.

The solid-state structure of cationic **Rh6** is shown in Fig. 3. **Rh6** crystallizes in the monoclinic space group $P2_1/n$ with a = 718.10 pm, b = 1926.95(18) pm, c = 2509.9(2) pm, α = 90°, β = 98.181(2)°, γ = 90°, Z = 4. The Rh-center adopts a three-legged-piano-stool-type geometry, too. The bite angle C(1)–Rh(1)–N(3) is 84.0° and the RH-NHC distance of 200.9(5) pm is virtually identical to the one found in **Rh5**. Notably, as in **Rh5**, the quinoyl group coordinates to the metal in the solid state (Rh(1)–N(3) = 211.1(4) ppm).

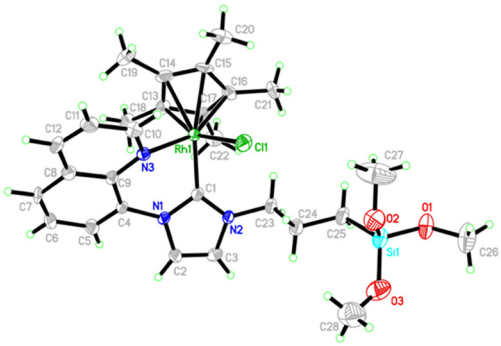

Fig. 3 Molecular structure of **Rh6** and selected bond lengths [pm] and angles [°]: Rh(1)–C(1) 200.9(5), Rh(1)–N(3) 211.1(4), Rh(1)–C(13) 213.2(6), Rh(1)–C(16) 216.1(6), Rh(1)–C(17) 217.0(6), Rh(1)–C(15) 221.8(5), Rh(1)–C(14) 221.7(6), Rh(1)–Cl(1) 239.60(15); C(1)–Rh(1)–N(3) 84.0(2), C(1)–Rh(1)–Cl(1) 92.21(16), N(3)–Rh(1)–Cl(1) 89.63(13), C(13)–Rh(1)–Cl(1) 159.19(17), C(16)–Rh(1)–Cl(1) 97.82(18), C(17)–Rh(1)–Cl(1) 131.52(17), C(15)–Rh(1)–Cl(1) 95.38(17), C(14)–Rh(1)–Cl(1) 123.87(18). BF_4^- counter ion omitted for clarity.

Homogeneous catalysis and time-dependent selectivity

To rule out any isomerization reactions, conversion as well as the ratio of the different stereoisomers was determined by GC-MS.

Representative kinetic profiles for **Rh1** in the hydroboration of 1-octyne and phenylacetylene, respectively, are shown in Fig. 4. No isomerization was observed within experimental error. Reactivity studies were carried out using different substrates. Both Rh(III) complexes, **Rh5** and **Rh6**, which contain an NHC ligand bearing a bulky quinoyl substituent, showed relatively low reactivity. NHC-Rh(I) complexes exhibited moderate to high conversion. For instance, 80% of 1-octyne was converted after 4 h using 1 mol% of **Rh1** (Table 1, entry 1). **Rh4** showed even better reactivity. Full conversion was achieved within 1 h when using 1-octyne or ethynylcyclohexane as a substrate (Table 1, entries 8 and 42). **Rh4** with an N-chelating NHC significantly outperformed the cationic complex **Rh3**, which only converted 21% of 1-octyne after 4 h. Moreover, **Rh7** allowed for the complete conversion of 1-hexyn-6-ol and 3,3-dimethyl-1-butyne after 1 h (Table 1, entries 33 and 36). In the hydroboration of 1-octyne, 6-chloro-1-hexyne, 1-hexyn-6-ol, 3,3-dimethyl-1-butyne, and ethynylcyclohexane predominantly the α and $\beta(E)$ isomers formed with an α:E ratio between *ca.* 1 : 2 and 1 : 3 (Table 1). Almost no $\beta(Z)$ isomer (≤2%) or only minor amounts of this isomer (<27%) formed (Table 1).

Pore-selective immobilization of catalysts in OMS

Catalysts **Rh1**, **Rh4**, **Rh5**, and **Rh7** were selectively immobilized inside OMS with two different pore diameters, referred to as $OMS_{60Å}$ and $OMS_{35Å}$, following published protocols.[29,33–36] Briefly, the mesopores of OMS with an average pore diameter of 35 and 60 Å, respectively, were filled with Pluronics®, followed by reaction with hexamethyldisilazane (HMDS) to transform all silanol groups outside the mesopores into the corresponding trimethylsilyl ethers. After removal of the Pluronics® by extensive

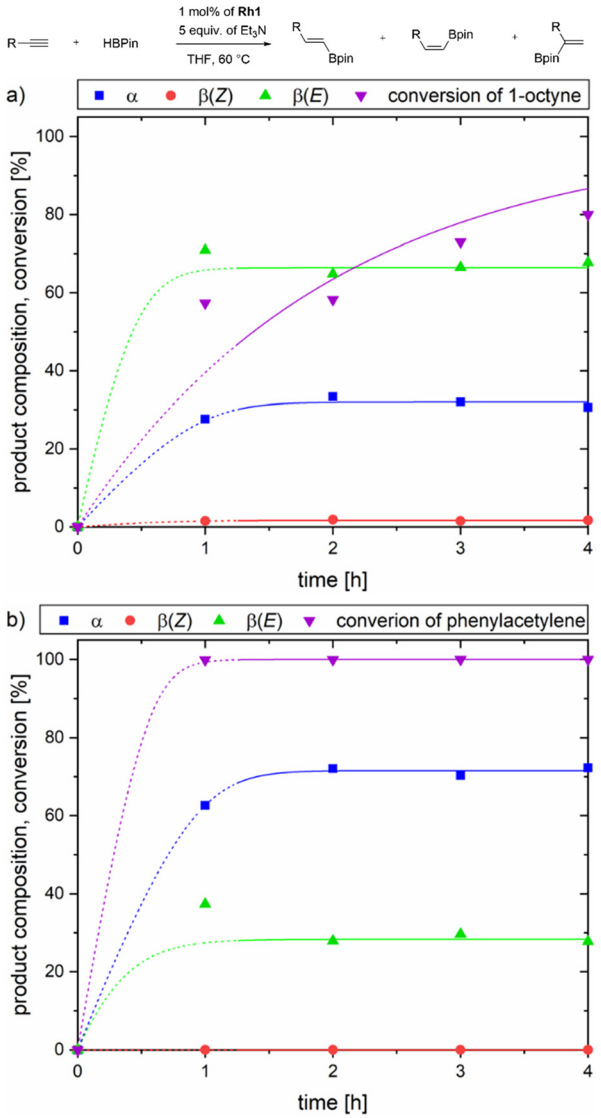

Fig. 4 Kinetic profiles of the hydroboration of 1-octyne (a) and phenylacetylene (b) at 60 °C using 1 mol% **Rh1** in THF. The lines were included to visually guide the reader.

Soxhlet extraction with ethanol, the corresponding catalysts were immobilized inside the mesopores. The Rh-content of the supported catalysts was determined by inductively-coupled plasma-optical emission spectroscopy (ICP-OES) and found to be 28.6, 26.1, 42.5, 49.3, 48.6, and 25.1 μmol g^{-1} for **Rh1@OMS$_{60Å}$**, **Rh1@OMS$_{35Å}$**, **Rh4@OMS$_{60Å}$**, **Rh4@OMS$_{35Å}$**, **Rh5@OMS$_{60Å}$**, and **Rh7@OMS$_{35Å}$**, respectively. Their reactivity in the hydroboration of 1-alkynes is summarized in Table 1. Only a moderate, yet significant improvement in *β*(*Z*) selectivity was observed. As observed in the related 1-alkyne hydrosilylation reactions,[29] higher *β*(*Z*)-selectivity was observed with OMS$_{35Å}$ as compared to OMS$_{60Å}$.

1-Alkyne hydroboration under SCILL conditions

"Solid catalyst with ionic liquid layer" (SCILL)[37–43] conditions here refer to catalysts covalently bound inside the mesopores of OMS$_{35Å}$ followed by coating of the corresponding immobilized catalyst with a very thin (*ca.* 1 nm) layer of an ionic liquid (IL), here [BMIM$^+$ BF_4^-] (Scheme 3). Such a thin layer of the IL translates into a low degree of pore filling (<40%). This way, **Rh1@SCILL**, **Rh4@SCILL**, and **Rh7@SCILL** were prepared and used in the hydroboration of 1-alkynes using methyl *t*-butyl ether (MTBE) as second, substrate-containing solvent that does not mix with the IL. For all aliphatic 1-alkynes investigated, a significant improvement in *β*(*Z*)-selectivity was observed (Table 1).

Particularly with **Rh1@SCILL$_{MTBE}$**, **Rh4@SCILL$_{MTBE}$**, and **Rh7@SCILL$_{MTBE}$** an increase in *β*(*Z*)-selectivity from 1–27% (homogenous) to 20–41% (SCILL$_{MTBE}$) was observed. In case THF was used as second solvent instead of MTBE, the increase in *β*(*Z*)-selectivity was even more pronounced; thus, the *β*(*Z*)-content in the hydroboration of 6-chloro-1-hexyne with **Rh4@SCILL$_{THF}$** and **Rh7@SCILL$_{THF}$** reached 67% (23% homogeneous) and 59% (6% homogeneous), respectively, rendering the *β*(*Z*)-isomer the predominant one. Next, a 1 nm coating of **Rh4@OMS$_{60Å}$** with BMIM$^+$ BF_4^- was performed and 6-chloro-1-hexyne was used as substrate. After 19 h, 51% of *β* (*Z*)-isomer was formed (67% in OMS$_{35Å}$), which shows that confinement persists, yet to a lesser extent. In fact, this was to be expected: confinement created by the 1 nm IL layer should exist for both materials, though to a lesser extent for larger pores, because of a reduced curvature inside these pores.

With 3,3-dimethyl-1-butyne, up to 54% of *β*(*Z*)-isomer formed using **Rh7@SCILL$_{THF}$**, whereas only 4% *β*(*Z*)-isomer were obtained using **Rh7** (Table 1, entries 36 and 38). A representative comparison of the selectivity under homogeneous, supported and SCILL conditions is shown in Fig. 5 for 6-chloro-1-hexyne and **Rh4**. Clearly, increasing confinement results in an increase in *β*(*Z*)-selectivity. Finally, in the hydroboration of terminal aromatic 1-alkynes a similar improvement in *β*(*Z*)-selectivity was observed, though to a far much lesser extent (Table S1). This is in line with the proposed mechanism: in contrast to the flexible alkyl chains, all aryl substituents sterically interfere with the *N*-(1-trimethoxysilylprop-3-yl)-group, rendering this transition state less favorable (Scheme 4).

Mechanistic aspects

Currently, the modified Chalk–Harrod-type mechanism is the widely accepted mechanism for the hydroboration of 1-alkynes, similar to what has been proposed for the transition metal-catalyzed hydrosilylation of 1-alkynes.[44–46] In some cases, also the formation of the overreduction product was reported.[3,11,29] In line with these reports, minor amounts (<10%) of the corresponding alkanes and corresponding alkynes were observed in our experiments by GC-MS, too. The proposed mechanism for a Rh(I) complex based on a chelating NHC (Scheme 4) involves the coordination of the alkyne to the metal center.

Table 1 Reactivity of **Rh1**, **Rh3**, **Rh4**, **Rh6**, **Rh7** and **Rh8** in the hydroboration of aliphatic terminal alkynes

#	Substrate	Catalyst	t [h]	Conversion (yield) [%]	$\alpha/\beta(Z)/\beta(E)$
1	1-Octyne	**Rh1**	4	80(80)	30/1/69
2	R = C_6H_{13}-	**Rh1@OMS$_{60Å}$**	25	26(26)	26/2/72
3		**Rh1@OMS$_{35Å}$**	24	80(78)	28/5/66
4		**Rh1@SCILL$_{MTBE}$**	4	59(55)	18/28/54
5		**Rh1@SCILL$_{MTBE}$**	24	>99(8)	18/27/55
6		**Rh1@SCILL$_{THF}$**	25	95(86)	14/39/47
7		**Rh3**	4	21(20)	22/23/55
8		**Rh4**	1	>99(87)	19/20/61
9		**Rh4@OMS$_{60Å}$**	23	>99(91)	15/27/58
10		**Rh4@OMS$_{35Å}$**	20	>99(84)	20/29/51
11		**Rh4@SCILL$_{MTBE}$**	20	>99(88)	16/34/50
12		**Rh4@SCILL$_{THF}$**	21	>99(91)	10/43/47
13		**Rh6**	4	13(12)	32/3/65
14		**Rh7**	2	58(55)	29/10/61
15		**Rh7@OMS$_{35Å}$**	20	31(25)	19/30/53
16		**Rh7@SCILL$_{MTBE}$**	20	64(56)	18/28/54
17		**Rh7@SCILL$_{THF}$**	18	49(41)	12/48/40
18		**Rh8**	2	58(53)	23/22/55
19	6-Chloro-1-hexyne	**Rh1**	1	25(25)	33/2/65
20	R = 4-Cl-C_4H_9-	**Rh1@SCILL$_{MTBE}$**	4	45(43)	24/16/60
21		**Rh1@SCILL$_{MTBE}$**	22	54(51)	22/26/52
22		**Rh1@ SCILL$_{THF}$**	25	47(45)	19/35/46
23		**Rh4**	1	42(40)	25/23/52
24		**Rh4@OMS$_{35Å}$**	22	50(46)	29/17/54
25		**Rh4@SCILL$_{MTBE}$**	20	78(73)	15/41/44
26		**Rh4@SCILL$_{THF}$**	16	93(89)	8/67/25
27		**Rh4@SCILL$^*_{THF}$**	19	31(29)	12/51/36
28		**Rh7**	1	37(35)	37/7/56
29		**Rh7@OMS$_{35Å}$**	23	51(46)	34/10/56
30		**Rh7@SCILL$_{MTBE}$**	20	33(30)	18/28/54
31		**Rh7@SCILL$_{THF}$**	18	48(45)	9/59/32
32		**Rh8**	2	58(55)	23/22/55
33	1-Hexyn-6-ol	**Rh7**	1	>99(99)	18/27/55
34	R = 4-OH-C_4H_9-	**Rh7@SCILL$_{MTBE}$**	25	>99(99)	18/34/48
35		**Rh7@SCILL$_{THF}$**	20	>99(99)	14/49/37
36	3,3-Dimethyl-1-butyne	**Rh7**	1	>99(98)	10/4/86
37	R = *t*Bu-	**Rh7@SCILL$_{MTBE}$**	22	>99(98)	2/24/74
38		**Rh7@SCILL$_{THF}$**	20	>99(99)	3/51/46
39	Ethynylcyclohexane	**Rh1**	2	42(41)	12/2/86
40	R = cyclohexyl-	**Rh1@SCILL$_{MTBE}$**	24	60(58)	15/20/65
41		**Rh1@SCILL$_{THF}$**	25	83(80)	13/33/54
42		**Rh4**	1	>99(98)	22/1/77
43		**Rh4@OMS$_{35Å}$**	22	92(89)	16/20/64
44		**Rh4@SCILL$_{MTBE}$**	20	98(86)	13/28/59
45		**Rh4@SCILL$_{THF}$**	22	98(91)	7/61/32
46		**Rh7**	3	59(58)	22/6/72
47		**Rh7@OMS$_{35Å}$**	23	51(50)	18/16/67
48		**Rh7@SCILL$_{MTBE}$**	20	52(50)	16/20/63
49		**Rh7@SCILL$_{THF}$**	22	58(56)	7/63/30

Reaction conditions: THF, 60 °C, 1 mol% catalyst loading, 10 mg of **Rh@OMS$_{60Å}$**, 12 mg of **Rh@OMS$_{35Å}$**, 12 mg of **Rh@SCILL$_{MTBE}$** (OMS$_{35Å}$ with 1 nm film of BMIM$^+$ BF_4^- and MTBE as a solvent), 12 mg of **Rh@SCILL$_{THF}$** (OMS$_{35Å}$ with 1 nm film of BMIM$^+$ BF_4^- and THF as solvent) or **Rh@SCILL$^*_{THF}$** (OMS$_{60Å}$ with a 1 nm film of BMIM$^+$ BF_4^- and THF as solvent), 1.5 eq. of HBpin, 5 equiv. of Et_3N as a base. *n*-Dodecane was used as internal standard. Conversion was determined by GC-MS; yields and the ratio of isomers were calculated from ^{1}H NMR (400 MHz).

Alkyne insertion and [1,3-*H*] shift then yields an alkenylidene intermediate followed by the oxidative addition of the alkylborane and, finally, the elimination of the $\beta(E, Z)$ hydroboration products. The observed α-product can be explained by a pathway that again starts with an alkyne insertion, followed by the oxidative addition of the alkylborane and formation of a 2-boryl-2-*R*-alkenylidene. H-Migration then reforms the catalyst under concomitant formation of the α-product. Unlike in the hydrosilylation of 1-alkynes by Rh(I) NHC complexes,[29] confining the catalyst inside ordered mesoporous silica (OMS) did not significantly improve $\beta(Z)$-selectivity. However, use of these supported catalysts under SCILL conditions allowed for much higher $\beta(Z)$-selectivity. For [BMIM$^+$][BF_4^-], molecular dynamics (MD) simulations revealed that the [BMIM$^+$] cations exhibit a preferred orientation in a thin, supported layer, where the

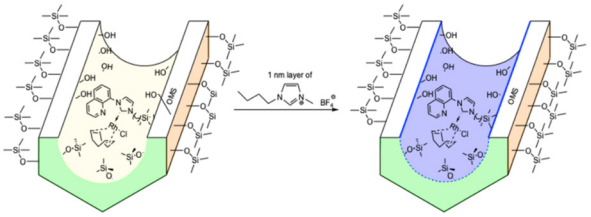

Scheme 3 Selective immobilization of **Rh1** inside OMS and realization of the SCILL conditions. Blue: thin (*ca.* 1 nm) film of [BMIM$^+$ BF$_4^-$].

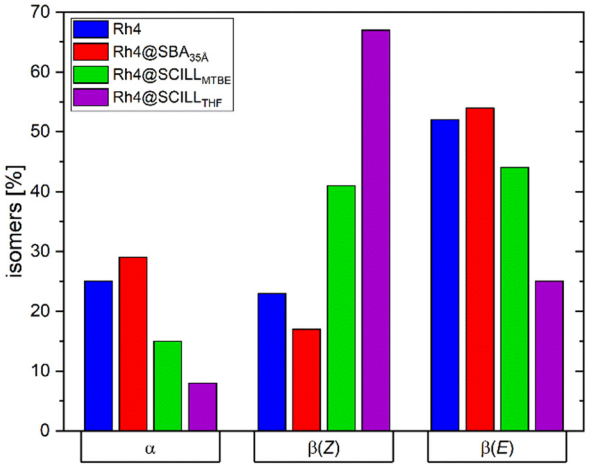

Fig. 5 Representative comparison of the selectivity in the hydroboration of 6-chloro-1-hexyne by the action of **Rh4** under homogeneous, supported and SCILL conditions.

methyl group and butyl tail point towards the silica wall and pore center, respectively, and the imidazolium moiety aligns with the surface.[47–51]

At 300 K this results in a cation and anion motion that is roughly by two orders of magnitude slower at the surface as in the bulk IL. Consequently, self-diffusion and structural relaxation processes are also much slower at the pore wall than in the bulk IL. This leads to a highly dense and ordered (quasi-solid) [BMIM$^+$][BF$_4^-$] layer at the silica surface of *ca.* 1 nm in thickness that is characterized by a very low mobility of the (ionic) species. Together with an N-chelating NHC, this confinement can be used to stabilize transition states, which ultimately allows for tuning the selectivity of the catalyst.[52] Thus, it is reasonable to assume that like in the solid-state structure of **Rh5** and **Rh6** but also in other N-chelated Rh-NHC complexes,[53] the quasi-frozen IL favors N-coordination of the quinoyl-moiety to the Rh-center, thereby restricting the rotation of the NHC of the confined catalyst. This favors the formation of the *β*(*Z*)-isomer since the corresponding Rh–vinyl complex with the boryl and the R-group in a *Z*-configuration has the least steric interaction with the 3-trimethoxysilylprop-1-yl group. Such joint action of a coordinating quinoyl group and the restricted mobility in a thin IL is further supported by the data obtained with **Rh4**, in which the NHC is tethered to Rh and which shows one of

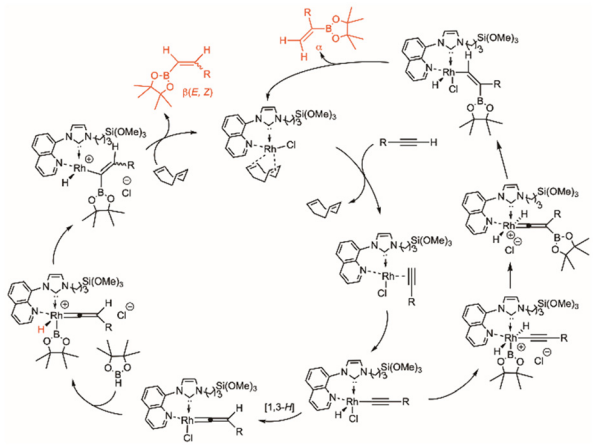

Scheme 4 Proposed hydroboration mechanism for a Rh(I) NHC complex.

the highest *β*(*Z*)-selectivities in all reactions, including the homogeneous ones. The observed increase in *β*(*Z*)-selectivity when changing from MTBE to THF can be rationalized by the fact that in contrast to MTBE, THF is slightly soluble in the IL and forms a solvent cage around the metal. This *solvent cage effect*[37] created by THF additionally increases confinement and stabilizes the transition state. The proposed mechanism also allows for a tentative explanation as to why *β*(*Z*)-selectivity was much lower with aromatic alkynes. In case R = aryl in Scheme 4, the intermediary cationic Rh–vinyl compounds are much better resonance stabilized than the corresponding Rh-vinyl compounds in which R = alkyl. It is therefore reasonable to assume that for R = aryl, decoordination of the quinoyl group is more likely to occur, which in turn allows the NHC ligand to rotate around the Rh–C^2-bond, thereby eliminating the steric interactions between the R-group and the 3-trimethoxysilylprop-1-yl moiety to a much larger extent.

3. Conclusion

Novel Rh(I) and Rh(III) complexes based on chelating NHCs were synthesized and tested in the hydroboration of terminal aliphatic alkynes with HBpin. Under homogenous conditions, the complexes showed selectivity towards the formation of the *α*- and *β*(*E*)-isomers. Immobilization of the catalyst inside the mesoporous material OMS$_{60Å}$ and OMS$_{35Å}$ slightly increased *β*(*Z*) selectivity, which was substantially increased up to 67% by applying SCILL conditions. Results are rationalized by a confinement effect particularly generated under SCILL conditions, which together with the chelating NHCs ultimately affects the transition states, thereby favoring the formation of the kinetic *β*(*E*)-isomer.

Author contributions

Boshra Atwi: formal analysis, investigation, visualization, writing-original draft. Dongren Wang: formal analysis, Johanna R.

Bruckner: resources, Wolfgang Frey: formal analysis, Michael R. Buchmeiser: conceptualization, funding acquisition, supervision, writing-original draft.

Conflicts of interest

The authors declare no competing financial interests.

Data availability

Primary data for this article (NMR spectra, kinetic measurements, and chromatograms) are available at the Data Repository of the University of Stuttgart (DARUS) [**https://darus.uni-stuttgart.de**] in connection with the DOI of the published paper.

Further data (experimental details, chromatograms, NMR and GC-MS spectra, crystallographic details for all catalysts) supporting this article have been included as part of the supporting information (SI). Supplementary information: experimental procedures and spectral data. See DOI: **https://doi.org/10.1039/d5cy00860c**.

CCDC 2468319–2468321 (**Rh6**, **Rh5** and **Rh3**) contain the supplementary crystallographic data for this paper.[54a–c]

Acknowledgements

Financial support by the Deutsche Forschungsgemeinschaft DFG (German Research Foundation, project ID 358283783 – SFB 1333/2 2022) is gratefully acknowledged. This research was also supported by the Ministry of Science, Research and the Arts Baden-Württemberg (Margarete von Wrangell program). Finally, we wish to thank Mr. Sarthak Mohanty for help with ICP-OES measurements.

Notes and references

1 M. P. Nunes, D. V. Jawale, F. G. Delolo, M. H. Araujo, E. Gravel, E. Doris and E. N. da Silva Junior, *Chem. Commun.*, 2023, **59**, 2763–2766.
2 J. Carreras, A. Caballero and P. J. Perez, *Chem. – Asian J.*, 2019, **14**, 329–343.
3 J. Bhattacharjee, A. Harinath, K. Bano and T. K. Panda, *ACS Omega*, 2020, **5**, 1595–1606.
4 K. Yamamoto, Y. Mohara, Y. Mutoh and S. Saito, *J. Am. Chem. Soc.*, 2019, **141**(43), 17042–17047.
5 A. K. Jaladi, H. S. Choi and D. K. An, *Nouv. J. Chim.*, 2020, **44**(32), 13626–13632.
6 K. Burgess and W. A. van der Donk, *Organometallics*, 1994, **13**(9), 3616–3620.
7 Y. Lyu, N. Toriumi and N. Iwasawa, *Org. Lett.*, 2021, **23**(23), 9262–9266.
8 S. Harder and J. Spielmann, *J. Organomet. Chem.*, 2012, **698**, 7–14.
9 J. F. Hartwig and C. N. Muhoro, *Organometallics*, 2000, **19**(1), 30–38.
10 J. Cid, J. J. Carbó and E. Fernández, *Chem. – Eur. J.*, 2012, **18**(5), 1512–1521.
11 E. Nieto-Sepulveda, A. D. Bage, L. A. Evans, T. A. Hunt, A. G. Leach, S. P. Thomas and G. C. Lloyd-Jones, *J. Am. Chem. Soc.*, 2019, **141**(46), 18600–18611.
12 J. Wen, Y. Huang, Y. Zhang, H. Grutzmacher and P. Hu, *Nat. Commun.*, 2024, **15**(1), 2208.
13 S. Jin, J. Li, K. Liu, W.-Y. Ding, S. Wang, X. Huang, X. Li, P. Yu and Q. Song, *Nat. Commun.*, 2022, **13**(1), 3524.
14 M. Yang, Y. Yu, W. Ma, Y. Feng, G. Zhang, Y. Wu, F. Zhou, Y. Yang and D. Liu, *RSC Adv.*, 2022, **12**(16), 9815–9820.
15 J. Carreras, A. Caballero and P. J. Pérez, *Chem. – Asian J.*, 2019, **14**(3), 329–343.
16 M. Haberberger and S. Enthaler, *Chem. – Asian J.*, 2013, **8**(1), 50–54.
17 S. Pereira and M. Srebnik, *Tetrahedron Lett.*, 1996, **37**(19), 3283–3286.
18 P. Andruszak, P. Pawluć, M. Kubicki and M. Zaranek, *J. Catal.*, 2025, **442**, 115888.
19 Z.-L. Wu, X. Lan, N. Gao, X. Kang, Z. Wang, T. Hu and B. Zhao, *J. Catal.*, 2021, **404**, 250–257.
20 K. L. E. Hale, D. D. Roberts and M. G. McLaughlin, *Eur. J. Org. Chem.*, 2025, **28**(11), e202401355.
21 H. Jang, A. R. Zhugralin, Y. Lee and A. H. Hoveyda, *J. Am. Chem. Soc.*, 2011, **133**(20), 7859–7871.
22 S. J. Geier, C. M. Vogels, J. A. Melanson and S. A. Westcott, *Chem. Soc. Rev.*, 2022, **51**(21), 8877–8922.
23 M. A. Iqbal, X. Yan, R. Li, F. Zhijia, S. Zhang and X. Li, *New J. Chem.*, 2024, **48**(7), 3149–3155.
24 C. Gunanathan, M. Hölscher, F. Pan and W. Leitner, *J. Am. Chem. Soc.*, 2012, **134**(35), 14349–14352.
25 N. K. Meher, M. Suryavansi and K. Geetharani, *Org. Lett.*, 2024, **26**(27), 5862–5867.
26 T. Ohmura, Y. Yamamoto and N. Miyaura, *J. Am. Chem. Soc.*, 2000, **122**(20), 4990–4991.
27 J. Liu, C. Wu, T. Hu, W. Yang, Y. Xie, Y. Shi, Q. Liu, Y. Shao and F. Zhang, *J. Org. Chem.*, 2022, **87**(5), 3442–3452.
28 A. K. Jaladi, H. S. Choi and D. K. An, *New J. Chem.*, 2020, **44**(32), 13626–13632.
29 P. K. R. Panyam, B. Atwi, F. Ziegler, W. Frey, M. Nowakowski, M. Bauer and M. R. Buchmeiser, *Chem. – Eur. J.*, 2021, **27**(68), 17220–17229.
30 S. Nath, S. Baguli and D. Mukherjee, *Organometallics*, 2024, **43**(20), 2458–2465.
31 S. Baguli, S. Chakraborty, S. Nath and D. Mukherjee, *Chem. – Eur. J.*, 2025, **31**(17), e202404659.
32 S. Denizaltı, H. Türkmen and B. Çetinkaya, *Tetrahedron Lett.*, 2014, **55**(30), 4129–4132.
33 J. R. Bruckner, J. Bauhof, J. Gebhardt, A.-K. Beurer, Y. Traa and F. Giesselmann, *J. Phys. Chem. B*, 2021, **125**(12), 3197–3207.
34 F. Ziegler, H. Kraus, M. J. Benedikter, D. Wang, J. R. Bruckner, M. Nowakowski, K. Weißer, H. Solodenko, G. Schmitz and M. Bauer, *et al.*, *ACS Catal.*, 2021, **11**(18), 11570–11578.
35 J. R. Bruckner, J. Bauhof, J. Gebhardt, A.-K. Beurer, Y. Traa and F. Giesselmann, *J. Phys. Chem. B*, 2021, **125**(12), 3197–3207.

36 F. Ziegler, J. Teske, I. Elser, M. Dyballa, W. Frey, H. Kraus, N. Hansen, J. Rybka, U. Tallarek and M. R. Buchmeiser, *J. Am. Chem. Soc.*, 2019, **141**(48), 19014–19022.
37 C. Li, H. Cai, B. Zhang, W. Li, G. Pei, T. Dai, A. Wang and T. Zhang, *Chin. J. Catal.*, 2015, **36**(9), 1638–1646.
38 M. Lijewski, J. M. Hogg, M. Swadźba-Kwaśny, P. Wasserscheid and M. Haumann, *RSC Adv.*, 2017, **7**(44), 27558–27563.
39 D. Kremitzl, K. Röhrs, M. B. Williams, P. S. Schulz and P. Wasserscheid, *J. Mol. Liq.*, 2024, **4**(1), 100092.
40 C. P. Mehnert, *Chem. – Eur. J.*, 2005, **11**(1), 50–56.
41 L. Winter, S. Trzeciak, C. C. Fernández, S. Massicot, T. Talwar, F. Maier, D. Zahn and H.-P. Steinrück, *ACS Catal.*, 2023, **13**(16), 10866–10877.
42 M. George, G.-R. Zhang, N. Schmitt, K. Brunnengräber, D. J. S. Sandbeck, K. J. J. Mayrhofer, S. Cherevko and B. J. M. Etzold, *ACS Catal.*, 2019, **9**(9), 8682–8692.
43 G.-R. Zhang and B. J. M. Etzold, *Adv. Funct. Mater.*, 2021, **31**(28), 2010977.
44 A. J. Chalk and J. F. Harrod, *J. Am. Chem. Soc.*, 1965, **87**(1), 16–21.
45 M. Reboli and M. Durandetti, *ChemCatChem*, 2025, **17**(10), e202402136.
46 D. A. Evans, G. C. Fu and B. A. Anderson, *J. Am. Chem. Soc.*, 1992, **114**(17), 6679–6685.
47 T. Pal, C. Beck, D. Lessnich and M. Vogel, *J. Phys. Chem. C*, 2018, **122**, 624–634.
48 S. Perkin, *Phys. Chem. Chem. Phys.*, 2012, **14**, 5052–5062.
49 M. Foroutan, S. M. Fatemi and F. Esmaeilian, *Eur. Phys. J. E: Soft Matter Biol. Phys.*, 2017, **40**, 19.
50 F. Borghi and A. Podestà, *Adv. Phys.:X*, 2020, **5**, 1736949.
51 R. Köster and M. Vogel, *J. Chem. Phys.*, 2022, **156**, 074501.
52 A. Böth, F. Kaltwasser, C. Priedigkeit, B. Atwi, W. Frey, M. R. Buchmeiser and U. Tallarek, *Catal. Sci. Technol.*, 2025, 4012–4023.
53 P. K. R. Panyam and M. R. Buchmeiser, *Faraday Discuss.*, 2023, **244**, 39–50.
54 (*a*) CCDC 2468319: Experimental Crystal Structure Determination, 2025, DOI: **10.5517/ccdc.csd.cc2nvh67**; (*b*) CCDC 2468320: Experimental Crystal Structure Determination, 2025, DOI: **10.5517/ccdc.csd.cc2nvh78**; (*c*) CCDC 2468321: Experimental Crystal Structure Determination, 2025, DOI: **10.5517/ccdc.csd.cc2nvh89**.